Gas slug ascent in a stratified magma: implications of flow organisation and instability for Strombolian eruption dynamics

A. Capponi, M.R. James, S.J. Lane

Lancaster Environment Centre, Lancaster University, Lancaster, LA1 4YQ, UK

Corresponding author: Antonio Capponi, Lancaster Environment Centre, Lancaster University, LA1 4YQ, UK, a.capponi@lancaster.ac.uk

Abstract

The canonical Strombolian paradigm of a gas slug ascending and bursting in a homogenous low-viscosity magma cannot explain the complex details in eruptive dynamics recently revealed by field measurements and textural and geochemical analyses. Evidence points to the existence of high-viscosity magma at the top of the conduit of Strombolian-type volcanoes, acting as a plug. Here, new experiments detail the range of flow configurations that develop during the ascent and burst of a slug through rheologically stratified magma within a conduit. End-member scenarios of a tube fully filled with either high- or low-viscosity liquid bracket three main flow configurations: (1) a plug sufficiently large to fully accommodate an ascending gas slug. (2) A plug that can accommodate the intrusion of low-viscosity liquid driven by the gas expansion, but not all the slug volume, so the slug bursts with the nose in the plug whilst the base is still in the low-viscosity liquid. (3) Gas expansion is sufficient to drive the intrusion of low-viscosity liquid through the plug, with the slug bursting in the low-viscosity layer emplaced dynamically above the plug. We show that the same flow configurations are viable at volcanic-scale through a new experimentally-validated 1D model and 3D computational fluid dynamic simulations. Applied to Stromboli, our results demonstrate that the key parameters controlling the transition between each configuration are gas volume, plug thickness and plug viscosity. The flow processes identified include effective dynamic narrowing and widening of the conduit, instabilities within the falling magma film, transient partial and complete blockage of the conduit, and slug disruption. These complexities influence eruption dynamics and vigour, promoting magma mingling and resulting in pulsatory release of gas.

Keywords

plugged conduit; magma mingling; slug dynamics; conduit geometry; flow configurations; analogue experiments; flow modelling

1. Introduction

Strombolian eruptions are characterized by short impulsive events. These typically occur in basaltic or andesitic magmas where viscosity is sufficiently low to allow gas segregation over short time scales (Blackburn et al., 1976; Parfitt, 2004; Houghton and Gonnermann, 2008). Explosions are interpreted as representing the arrival and burst of over-pressured large gas pockets (slugs) at the surface (Chouet et al., 1974; Blackburn et al., 1976). The slugs can form either by coalescence of smaller bubbles at geometrical discontinuities in the conduit (Vergniolle and Jaupart, 1986; Jaupart and Vergniolle, 1988) or by differential ascent rate of the bubbles with respect to the magma column (Parfitt and Wilson, 1995; Parfitt, 2004). Either way, the ascent, expansion and burst of slugs have almost always been considered in rheologically uniform media (e.g., Vergniolle and Brandeis, 1996; Vergniolle et al., 1996; Seyfried and Freundt, 2000; James et al., 2006, 2008; Kobayashi et al., 2010; Del Bello et al., 2012; Lane et al., 2013).

However, an increasing body of evidence (e.g., Lautze and Houghton, 2005, 2006; Polacci et al., 2009; D'Oriano et al., 2010; Colò et al., 2010; Gurioli et al., 2014) suggests that the cooling, degassing and crystallisation of the uppermost part of the magma column, along with mixing with recycled material from collapses of the conduit wall, re-entrained pyroclasts and lithics, could generate an evolved magma region at the top of the conduit. Gas slugs must ascend and burst through this stratified rheological heterogeneity. The rheological properties and thickness of this region may influence explosion intensity and style (Lautze and Houghton, 2005, 2006), while textural and geochemical variations in the ejecta may reflect mingling of magmas with different physical properties in the shallow conduit (Polacci et al., 2009; D'Oriano et al., 2010; Colò et al., 2010; Gurioli et al., 2014). Textural features observed in samples collected at Stromboli seem to correlate with explosion frequency and magnitude, with a broader mingling promoted by increased magma and gas flux (i.e., greater explosion frequency and vigour). In contrast, a lower flux (i.e., low level of activity) leads to more restricted mingling (Lautze and Houghton, 2006). Complexities in eruptive dynamics, such as pulses within a single Strombolian eruption (Taddeucci et al., 2012; Gaudin et al., 2014), are also difficult to explain with simplified models of slug burst in a rheologically uniform fluid, although conduit discontinuities could play a role (James et al., 2006).

Such evidence motivated initial experimental work on the effects of a viscous upper layer (or 'plug') on eruptive dynamics (Del Bello et al., 2015). In this scenario, a gas slug ascending and expanding in a column of low-viscosity liquid overlaid by a plug drives an intrusion of low-viscosity liquid into the plug. The plug liquid thus creates a viscous annulus that, in turn, encloses the intrusion (Fig. 1). As the slug arrives at the plug base, it uses the low-viscosity intrusion to rise through the plug. The slug can burst in two different flow configurations: 1) whilst fully accommodated into the plug volume, or 2) whilst in a low-viscosity layer emplaced by the intrusion above the plug. Each configuration encompasses apparent dynamic narrowing and widening of the conduit for the slug, instabilities within the falling film surrounding the slug, transient partial blockages of the conduit, and slug disruption (Del Bello et al. 2015). These complexities gave insight into the generation of eruptive pulses and mingled pyroclasts, together with enhancement of slug overpressure with respect to a single-viscosity system (Del Bello et al., 2015); however, accurate scaling for slug expansion and viscosity contrast was not achieved.

Here, we build on the experimental foundation of Del Bello et al. (2015) to fully define the rich range of fundamental fluid configurations that can develop in association with slug flow through a viscous plug at the top of a volcanic conduit. We used comprehensively scaled laboratory experiments to identify flow organisation and instability within different fluid configurations expressed by varying relative plug and slug sizes. We developed a model to determine these configurations for a given set of parameters, and validated it against the laboratory data and, at volcano-scale, against the results of 3D computational fluid dynamics simulations. Finally, we explored the implications of flow richness in the shallow conduit for interpretation of Strombolian eruptive processes.

2. Methods

The complex volcanic system was simplified to explore the effect of a vertical rheology contrast on the behaviour of the slug during its ascent, expansion and burst in a constant-geometry tube filled with Newtonian liquids. The experimental apparatus (Fig. 1) comprised a vertical 3-m-high glass tube with internal diameter D of 0.025 m. The base of the tube was sealed, with the exception of the gas injection system. The top was connected to a vacuum chamber in order to reduce the ambient pressure, P_a, and enable slug expansion processes to be scaled (James et al., 2008). We used *AS100* silicone oil (viscosity μ = 0.1 Pa s, density ρ = 990 kg/m^3, Wacker Chemie AG) as analogue for low-viscosity magma (Table 1), improving on the experiments of Del Bello et al. (2015) by (a) providing more accurate scaling of viscosity contrast, and (b) enabling access to the explosive region of slug expansion (James et al., 2009; Del Bello et al., 2012). Immiscible castor oil (μ = ~1 Pa s, ρ = 961 kg/m^3) represented the high-viscosity plug with a density less than that of the silicone oil and a suitably high viscosity. At both laboratory and volcanic scales, surface tension plays a negligible role (e.g., Seyfried and Freund, 2000), and the inverse viscosity N_f controls the ascent of a slug:

$$N_f = (\rho/\mu)\sqrt{gD^3} \quad (1),$$

where g is the gravitational acceleration. For the tube geometry, we obtain N_f values of ~12 and ~122 for the castor oil and silicone oil respectively (Table 1). These values lie in regions of the flow regime where the slug behaviour is controlled by viscosity in the plug, and by inertia with viscous contributions in the silicone oil (e.g., White and Beardmore, 1962).

The apparatus was filled to a height of ~1.43 m with either silicone oil only, or with silicone oil overlain by a layer of castor oil. Layer thickness of the plug was non-dimentionalised as a function of the tube diameter, D: ~2.5 (1D), ~5 (2D), ~12.5 (5D), ~25 (10D) and ~50 (20D) cm plugs, widening the range of Del Bello et al. (2015), which only considered ~5 (2D) and ~17.5 (7D) cm layers. In addition to the gas volumes (2, 4, 6, 8 and 10 ± 0.1 ml) and P_a (P_a = 3 kPa, limited by water boiling point) used in Del Bello et al. (2015), we injected volumes of air (V_0) of 17, 24, 32 and 49 ± 0.1 ml, with P_a reduced to 1 ± 0.1 kPa and 300 ± 0.1 Pa, greatly extending the range of gas expansion ratios.

The injected gas volumes non-dimensionalise through the parameter V_a' (Del Bello et al. 2012; Supplementary Content), giving V_a' = 0.08–2, 0.6–14 and 6–152 for experimental P_a of 3 kPa, 1 kPa and 300 Pa respectively. Scaled to the volcanic case, these values represent erupted gas volumes at atmospheric pressure of 4–90 m^3, 28–690 m^3 and 300–7300 m^3, and cover the range of gas volumes estimated for normal strombolian activity (Vergniolle and Brandeis, 1996; Vergniolle et al., 1996; Ripepe and Marchetti, 2002; Chouet et al., 2003; Harris and Ripepe, 2007; Mori and Burton, 2009) i.e., 2–2 × 10^4 m^3 (0.5–3000 kg), and for gas puffers, 50–190 m^3 (10–30 kg). Each experiment was imaged at 300 ± 0.1 frames per second with a Basler acA2000-340km high-speed camera.

To extend our 1D numerical model to volcanic-scale, we considered an idealised system with a 200-m-high magma column within a conduit of radius 1.5, 2 or 2.5 m, covering the range of values appropriate to Stromboli (Taddeucci et al., 2012; Gaudin et al., 2014). Magma viscosities range between 10–50 kPa s and 50–500 Pa s, with densities of 1300 kg/m^3 and 900 kg/m^3, for the plug and the underlying magma respectively (Gurioli et al., 2014). These parameters give N_f values ~4.55 to ~0.42 for the plug and ~630 to ~29 for the underlying magma. Slug ascent is under dominant viscous control in the plug, but with a significant degree of inertial contribution within the underlying magma, a condition mimicked experimentally.

3. Results

The experiments revealed a rich set of flow configurations, reflecting variation in the ratio of the lengths of the high-viscosity plug and gas slug. The flow configurations can be conceptually considered within a spectrum of relative plug lengths, ranging from infinite (i.e. a conduit fully filled with the high-viscosity liquid) to zero (i.e. a conduit filled with the low-viscosity liquid). These single-viscosity end-members bracketed three distinct intermediate and more complex flow configurations. The transitions between these configurations were not sharp, and included intermediate behaviours. However, they encompassed the same processes observed in the main configurations and, thus, are not detailed here (see Supplementary Content for more information).

3.1. Single viscosity

We define infinitely thick and infinitely thin plugs as end-member configurations (Fig. 2a, e) in which slug ascent is effectively within a single-viscosity system. In the experiments, the injection of air at the base of the apparatus formed a slug (James et al., 2008; Lane et al., 2013; Del Bello et al., 2015) that rose, expanded and elongated surrounded by a falling liquid film. The slug burst when all the liquid head above it has flowed into the falling film, except for a thin layer forming a meniscus. When ascending in a low-viscosity liquid (Fig. 2e), the slug occupied almost all the cross sectional area of the tube, surrounded by a thin falling film of liquid (Fig. 3); for gas volumes larger than 17 ml, film instabilities developed with time. At burst, the meniscus ruptured, and its remnants were dragged upward by the released gas before falling or draining back on the liquid surface (Video V01). Small volumes of gas (2-8 ml) produced pre-burst oscillation of the slug nose at surface.

For slug ascent in high-viscosity liquids (Fig. 2a), the slug ascended with a lower velocity, surrounded by a thicker falling film, thus the fraction of the tube cross-section occupied by the film, *A'* (Del Bello et al., 2012; Supplementary Content), increased from ~0.41 to ~0.52 (Table 1, Fig. 3). Consequently the area of the tube occupied by the slug decreased, while its length increased. The rate of gas expansion was slower, driving a slower acceleration of the liquid surface. When at the liquid surface, the slug burst with a slow rupture of a thick viscous meniscus, which completely drained to the tube wall just above the burst point and without the ejection of any droplets or observable pre-burst oscillation.

3.2. Configuration 1

In a layered system in which the plug volume was significantly greater than the slug volume, a steady slug flow was established in both the low- and high-viscosity liquids (Fig. 2b), with a transitional period as the slug moved between the fluids (Video V02, 8-13 s). At the onset of an experiment the slug rose in the low-viscosity liquid. As it ascended, gas expansion drove an intrusion of low-viscosity oil into the plug, the extent of which depended on the relative volumes of the slug expansion and the plug. Around the intrusion, the high-viscosity liquid represented a viscous annulus, with an average radial thickness ∼4 mm, thinnest at the plug base (Fig. 3).

When the nose of the ascending slug reached the base of the annulus, the annulus acted as a dynamic change in the confining geometry. This forced the slug to ascend through a diameter reduction and into the intrusion (Fig. 4a, sketch II; Video V02, 8 s). For all configurations the intrusion volume must equal the slug volume expansion; therefore the intrusion was always smaller than the slug itself. Thus, at some point, the slug transited from ascending within the intrusion to within the main body of the plug itself, defining Configuration 1. Once this was complete, the high-viscosity plug liquid fully accommodated the bubble within it (Fig. 4a, sketch III). Ascent rate and slug morphology became more viscously dominated and burst processes reflected those in high-viscosity fluids (Video V02).

3.3. Configuration 2

For experiments in which the plug volume was insufficient to fully accommodate the slug, slug burst occurred with the slug nose within the plug liquid, and the slug base still in the low-viscosity liquid (Fig. 2c). As for Configuration 1, when the slug arrived at the base of the annulus, it used the intrusion as a pathway through the plug (Fig. 4b, sketch II; Video V03, 13-16 s) with, at some point, the slug nose entering the high-viscosity plug liquid (Fig. 4b, sketch III; Video V03, 16 s). At burst, the high-viscosity meniscus disrupted into small droplets (Video V03, 17 s). If the nose of the intrusion had almost reached the plug surface when the slug burst (mainly for 5*D* and 10*D* plugs and 10, 17 and 24 ml slugs), then the burst involved droplets of a mixture of low/high viscosity oil, ejected up the tube.

3.4. Configuration 3

Configuration 3 represents the scenario in which slug expansion is sufficiently large that the low-viscosity intrusion breaches the plug top and emplaces a layer of low-viscosity liquid above the annulus (Fig. 2d; Video V04, from 5 s onwards). Experimentally, the viscous annulus effectively generated two regions of geometry change for ascending slugs; at the base of the plug, the annulus created a dynamic restriction, whilst at the top, slugs passed back into the low-viscosity liquid only – effectively a dynamic widening (Fig. 4c, sketch II). The widening enabled the slug nose to accelerate and the abrupt change led to rapid draining of the liquid head around the slug (James et al., 2006). As the increased downward flux of liquid past the slug nose converged at the top of the annulus, the falling film thickened within the annulus, creating a narrowing neck around the slug. If this closed, the gas flow may be temporarily halted as the gas slug was broken into two (Fig. 3c, sketch III; Video V04, 16-18 s) or, if the processes were repeated, more offspring bubbles. The break-up process, always taking place in < 1 s after the main bubble burst, generated up to 4 offspring bubbles in the experiments, bursting sequentially. We observed also partial restrictions of the gas escape pathway, at a mean frequency of 2 per second.

When the slug nose within the intrusion ascended above the top of the annulus, instabilities formed in the falling film around the slug body due to the dynamic geometry change; these instabilities propagated down the low-viscosity film within the annulus and continuously disrupted the boundary between the two liquids, initiating mingling (Fig. 4c, sketch II-III). Sometimes, for large gas volumes and thin plugs (1*D* and 2*D*), gas expansion caused rapid intrusion of low-viscosity liquid breaking through the plug: some of the high-viscosity annulus was detached, dragged upward within the low-viscosity liquid above and surrounding the slug body, and mixed into the low-viscosity liquid. As burst progressed, pockets of this mingled mixture were ejected (Fig. 4c, sketch IV). The burst process was highly variable: it involved bubble oscillations and detachment of the entire meniscus, or bubbles burst without any oscillation, with a complete disruption of the meniscus and droplets ejected high in the tube and followed by several collapses of the film lining the tube wall (Video V04).

4. Determination of flow configurations at volcano-scale

To determine the flow configuration (e.g., 1 to 3) for a specific set of parameters, we developed a first-order 1D model to describe slug ascent, expansion and intrusion of liquid into the plug. The model is based on previously used geometrical representations of slug morphology (Vergniolle, 1998; Seyfried and Freundt, 2000; James et al., 2008, 2009; Del Bello et al., 2012) and, for simplicity, we neglected inertial forces on the liquid above the slug. Such inertial effects can be important when large rates of gas expansion are involved (James et al., 2008, 2009), but expansion rates will be generally reduced by the presence of the plug. Thus although the model will slightly overestimate gas expansion, this simplification is suitable for a model aimed only at estimating the active flow configurations. Furthermore, to retain the first-order approach and avoid the complexities involved with transitional behaviour and slug ascent within the intrusion, the model determines the active configuration no later than the point at which the slug nose reached the original plug base, without considering the full ascent up to slug burst.

The slug is represented as a cylinder of length L and constant radius r_s, ascending in a vertical tube of radius r_c (Fig. 5, Table 2 for notation). Above the slug, we consider three different sections; the lowest filled by the low-viscosity liquid only, viscosity μ_1 and density ρ_1, of height h_1. The uppermost section represents the viscous plug, with viscosity μ_2, density ρ_2, radius r_c and height h_3. The middle section represents the intrusion of low-viscosity liquid into the high-viscosity plug to form the annulus, with viscosity μ_1 and density ρ_1, length h_2 and radius r_ϕ. The radius r_ϕ is the result of $r_\phi = r_c - r_p$, where r_p is the thickness of the high-viscosity layer against the tube wall which forms the high-viscosity annulus. Due to the evolving nature of the annulus, r_p will vary in space and time. Consequently, in order to provide a characteristic first-order estimate in our straightforward model we assume a thickness as for a falling film surrounding a slug, which can be given as a function of the inverse viscosity, N_f (Llewellin et al., 2012; Supplementary Content):

$$r_p = \left(0.204 + 0.123 \tanh\left(2.66 - 1.15 \log_{10} N_f\right)\right) r_c \qquad (2).$$

Initial conditions are the height of the low-viscosity liquid above the slug nose, h_1', the height of the plug, h_3', the initial (magmastatic) bubble pressure, $P_0 = \rho g(h_1' + h_3') + P_a$, the slug length, L_0, and radius, $r_s = r_c - \lambda$, where λ is the thickness of the low-viscosity falling liquid film, determined by using equation (2) for the low-viscosity liquid (Fig. 3).

We assume constant velocity v_s for the slug base, thus, at any time, t, the height of the low-viscosity liquid column h_1 above the slug nose is given by:

$$h_1 = (L_0 - L) - v_s t + h_1' \qquad (3).$$

Equating the intrusion volume to the gas expansion, the height of the low-viscosity liquid intrusion h_2 can be expressed as:

$$h_2 = -A(L_0 - L) \quad (4),$$

where $A = \frac{r_s^2}{r_\phi^2}$. Conservation of volume for the plug liquid yields:

$$\pi r_c^2(h_3 + h_2) - \pi r_\phi^2 h_2 = \pi r_c^2 h_3' \quad (5),$$

where h_3 is the distance between the plug top and the intrusion (h_2) top. Simplifying and substituting for h_2, h_3 can be expressed as:

$$h_3 = h_3' + (L_0 - L)(A - B) \quad (6),$$

where $B = \frac{r_s^2}{r_c^2}$.

The force on the liquid column above the slug due to the pressure difference between the slug and the surface is given by $F_p = \pi r_s^2(P - P_a)$. If the slug behaves like a perfect gas and adiabatic expansion, then PV^γ = *constant* (where γ is the ratio of specific heat), and the slug pressure, with constant radius and pressure P_0 at $t = 0$, F_p can be expressed as:

$$F_p = \pi r_s^2\left(P_0 L_0^\gamma L^{-\gamma} - P_a\right) \quad (7).$$

The gravitational force is given by $F_g = -\pi r_s^2 \rho h g$, where ρ and h are respectively the density and the height of the involved liquid, and g is the acceleration due to gravity. Finally, assuming no-slip conditions at the wall, the Poiseuille law gives the viscous force for a laminar flow in a cylindrical pipe:

$$F_v = -8\pi\mu h V_f \quad (8),$$

where μ is the viscosity of the liquid and V_f the flow velocity. If we assume that the liquid flow is equal to the volume flux controlled by the gas expansion, we obtain:

$$F_v = -8\pi\mu h \dot{L} B \quad (9).$$

Equating the pressure force with the sum of the gravitational and viscous forces for the low-viscosity liquid column above the slug, the low-viscosity liquid intrusion, and the plug, we obtain:

$$\pi r_s^2\left(P_0 L_0^{\gamma} L^{-\gamma} - P_a\right) = -\pi r_s^2 \rho_1 g(h_1 + h_2) - \pi r_s^2 \rho_2 g h_3 - 8\pi \dot{L}\frac{r_s^2}{r_c^2}(\mu_1 h_1 + \mu_2 h_3) - 8\pi \dot{L}\frac{r_\phi^2}{r_c^2}\mu_1 h_2 \qquad (10).$$

Simplifying and substituting for both h_2 and h_3 yields:

$$(P_0 L_0^{\gamma} L^{-\gamma} - P_a) = -g[\rho_1(h_1 - A(L_0 - L))] - g[\rho_2(h_3' + (L_0 - L)(A - B))] - 8\dot{L}r_c^{-2}[\mu_1 h_1 + \mu_2[h_3' + (L_0 - L)(A - B)]] - 8\dot{L}r_\phi^2 \frac{r_c^{-2}}{r_s^2}\mu_1[-A(L_0 - L)] \qquad (11),$$

and finally:

$$\dot{L} = \{-g[\rho_1(h_1 - A(L_0 - L))] - g[\rho_2\left(h_3' + (L_0 - L)(A - B)\right)] + (P_0 L_0^{\gamma} L^{-\gamma} - P_a)\}/\{8r_c^{-2}\,[\mu_1 h_1 + \mu_2\,[h_3' + (L_0 - L)(A - B)]] + 8r_\phi^2 \frac{r_c^{-2}}{r_s^2}\mu_1\,[-A(L_0 - L)]\} \qquad (12).$$

The first order differential is solved numerically in *Matlab*, using a Runge-Kutta formula. With the focus of the model being to determine flow configurations within the parameter space of a system, it is sufficient to consider the values determined when either the intrusion breaches the plug surface, h_3 = 0 (indicating Configuration 3) or when the slug reaches the plug base, h_1 = 0. In this latter case, Configuration 1 is identified if there is sufficient plug material to fully encompass the volume of the gas slug, otherwise Configuration 2 is determined.

4.1. Model validation

To verify the suitability of equation (12), we compared modelled slug ascent to experimental data representative of each configuration (Fig. 6). For model inputs, we measured the ascent velocity of the base from the laboratory video, derived the initial slug length directly from the experimental gas volumes, and, to calculate the intrusion radius, assumed the value of the annulus radius equal to a falling film surrounding a slug. For Configuration 1 (Fig. 6a) and 2 (Fig. 6b), the model accurately reproduced the variations in position of the slug nose, base and the liquid surface, with the intrusion level always below the plug surface. For Configuration 3 (Fig. 6c), the model accurately predicted both the timing and position of the plug breach.

We neglected the inertial forces in the formulation of equation (12), so gas expansion is slightly overestimated by the model, as well as the intrusion volume, leading to small discrepancies between the laboratory experiments and model results (Fig. 7a). Larger slugs and rapid gas expansion, resulting in greater intrusion of low-viscosity liquid, cause the model prediction of Configuration 3 or 2 instead of Configuration 2 or 1 respectively. However, when compared to the experimental data and considering the simplifying assumptions, the model successfully identifies the dominant areas of parameter space for Configuration 1 and 3, separated by Configuration 2.

Applying the model to an idealised volcanic-scale scenario (Fig. 7b) indicated that a similar pattern of flow configurations could be relevant at Stromboli. To corroborate this, we carried out 3D computational fluid dynamics (CFD) simulations using the commercial software Flow3D (James et al., 2008; Chouet et al., 2010; Del Bello et al., 2015).

First, we modelled selected laboratory experiments to validate the CFD model against experimental data, recreating the same experimental conditions (apparatus geometry, injected slug volumes, experimental ambient pressures and plug thickness). The CFD simulations produced results similar to those observed in the laboratory in terms of both flow processes and slug and intrusion shapes (Fig. 8a, b; Video V05). The generation of the viscous annulus and the complex interaction between the two liquids were also accurately reproduced, together with the disruption of the slug and the generation of offspring bubbles and partial blockages of the conduit (fig. 8c, d; Video V05).

For the volcanic scenario, a 300-m-high vertical cylinder with a radius of 1.5 m (for CFD simulations, only this conduit radius was used), closed at the lower boundary, represented the conduit. Although a closed condition was not realistic and more representative of the experimental condition, once a stable slug flow was established in the conduit, this boundary condition did not affect the flow (e.g., James et al., 2008; Chouet et al., 2010). The 200-m-high magma column was modelled as an incompressible Newtonian liquid with a temperature-dependent viscosity and divided into two temperature regions. The first region covered the low-viscosity magma, while the second region defined the plug. Viscosity values ranged between 10-1000 Pa s for the magma beneath the plug and between 1-20 kPa s for the plug, lower than the typical value of Stromboli (1-50 kPa s, Gurioli et al., 2014): exceeding that range resulted in simulation initialisation problems. The gas slug was modelled as a continuous void region (contains no mass) governed by the equation $PV^{\gamma} = constant$.

The volcano-scale simulations, for plug thickness and gas volumes of 3–60 m and 30–250 m^3 respectively, showed changes in slug shape as it enters the annulus (Fig. 8e, f), and reproduced the generation of instabilities and slug disruption (Fig. 8g-l). As predicted, the slug transition from a low-viscosity magma to a viscous plug caused a sudden decrease in the slug ascent velocity. As for the burst process, different dynamics can be associated with the different configurations. Based purely on visual observation of the burst dynamics, Configuration 1 involved a slow fragmentation of the viscous meniscus above the slug, with almost no pyroclast ejection. In Configuration 2 the fragmentation of the magma meniscus was fast and its particles were ejected up to tens of meters above the burst point (note this is a minimum inertial height since no drag from expanding gas is applied). Configuration 3 explosions ranged in style depending on slug volumes, plug thickness, generation of secondary bubbles and blockages of the conduit. In general the burst process seemed characterized by dynamics common to both Configuration 1 and 2, with ejection of material above the burst point but at heights inferior to Configuration 2. Furthermore, most of the ejecta appeared to be mingled and collapsed back in the conduit, creating partial blockages that forced the slug into smaller pockets of gas.

The simulations, showing flow processes similar to those observed in the scaled laboratory experiments, support the applicability of the 1D model and endorse the main roles played by slug volume and plug properties in determining the prevailing flow configuration. The computational fluid dynamics simulations also enabled investigation of the role of the underlying magma viscosity on the complex syn- and post-burst dynamics involved in Configuration 3. A lower viscosity magma drained faster along the conduit/annulus walls, accumulating at the top of the annulus. This promoted the fast and cyclic creation of narrowing necks around the slug. Every time a neck closed, the slug was disrupted, generating offspring bubbles and secondary bursts (pulses). Magma clots were also ejected at greater heights and their collapse produced partial blockages of the conduit, trapping the slug gas into smaller pockets and leading to sub-pulses. For each pulse and sub-pulse, burst depth gradually increased (Video V06, 21-34 s). With increasing magma viscosity, drainage along the conduit walls slowed, with the generation of fewer, or no, pulses but only partial blockages due to collapse of material back into the conduit (Video V06).

5. Implications for Strombolian eruptions

Our experiments characterised the spectrum of flow configurations for a set of liquid parameters, tube geometry and for single slug ascent in a rheologically stratified conduit. In our idealised volcanic scenario, both configuration model and CFD simulations indicate the sensitivity of configurations to initial gas volumes and plug properties (Fig. 7b). For a particular conduit radius, the distribution of configurations in parameter space was insensitive to the viscosity of the magma beneath the plug, which can be considered mainly as a means of delivering the slug into the plug (Fig. 7b, Video V06). In contrast, conduit radius had a strong influence on configuration transitions. The Configuration 1 domain increased with increasing radius (Fig. 7b) implying that, for identical magmatic conditions, vents of different radius could erupt with different style.

Under plugged conditions, it appeared both experimentally and numerically that the burst vigour was always greater when compared to an unplugged scenario. As previous models in single-viscosity systems demonstrated, slug overpressure varies with the thickness of the falling film, controlled by magma viscosity (James et al., 2009; Del Bello et al., 2012). Hence, the same initial gas volume burst with a lower overpressure in a low-viscosity liquid (thin film, Fig. 2e) compared to in a higher viscosity liquid (thick film, Fig. 2a). This effect occurred in Configuration 1; however, because the slug was initially ascending in a low-viscosity magma, its overpressure also increased due to pressurization of the conduit below the plug. The greater the plug thickness and viscosity, the more pressure can be retained to be released during a more vigorous burst.

Within Configuration 2, gas expansion intruded a substantial volume of low-viscosity liquid into the plug; the further the intrusion penetrated, the higher the slug can ascend within the low-viscosity channel enclosed within the viscous annulus. The greater thickness of the complex “double” falling film resulted in increased slug lengthening to accommodate gas expansion, opposed by the presence of the un-intruded plug above, and enhancing the generation of overpressure. In Configuration 3, the full development of an open low-viscosity channel through the plug removed the ‘capping’ effect, allowing the slug to expand more freely and, compared to the other two configurations, reducing slug overpressure.

Furthermore, the partial constriction of the tube and the gas slug break-up into smaller pockets produced multiple bursts and modulation of the gas release within Configuration 3.

In support of the role of different flow configurations on slug overpressure, Del Bello et al. (2015) quantified similar effects for their experiments, that can be now categorised as Configurations 1 and 3 (Configuration 2 was not identified). All of their plugged experiments, regardless plug thickness, showed a greater acoustic amplitude and an increase in slug overpressure with respect to the single-viscosity experiments (Fig. 3 and 4 in Del Bello et al. 2015). In Configuration 1, Del Bello et al’s slugs showed a greater increase in both conduit pressurization during slug ascent and acoustic amplitude at burst compared to slugs bursting in Configuration 3. In Configuration 3, slugs were characterized by a lower overpressure but also by highly variable gas release rates, both in terms of magnitude and time, and generated a range of pressure pulses (burst of offspring bubbles) and sub-pulses (conduit constriction) (Del Bello et al. 2015).

Therefore, for volcanoes where multiple vents are constantly active (e.g., Stromboli and Yasur, Vanuatu), each active vent may be characterized by plugs with different properties, controlling both burst dynamics and explosion magnitude, thus affecting acoustic amplitudes. However, a unique explanation of a particular acoustic amplitude is further complicated because the same gas mass can lead to different flow configurations sensitive to conduit width (Fig. 7b). Slug parameterization and the linking of field results and fluid dynamic models, so far based on single-viscosity scenarios suggesting a positive correlation for the burst pressure with both initial slug volume and magma viscosity (e.g., Vergniolle and Brandeis 1996; James et al., 2009; Del Bello et al., 2012; Lane et al., 2013), becomes more poorly constrained with the added degrees of freedom provided by rheological complexity.

5.1. Magma mingling

As a result of interactions between the different viscosity magmas, the textural and geochemical properties of the ejected pyroclasts will also depend on the flow processes occurring within the plug. Our experiments reveal that mingling of material may occur in two ways. If the low-viscosity magma intrudes the plug deep enough but without breaching it, the slug approaches the surface surrounded by a low-viscosity magma film, enclosed in turn by the high-viscosity annulus forming a tri-axial flow (Del Bello et al., 2015), i.e., at the boundary of Configuration 2 with 3. At burst, the fragmenting meniscus will comprise layers of both low- and high-viscosity magma, promoting mingling and ejection of mingled pyroclasts. However, with only the meniscus region involved, mingling is expected to be a relatively localized process. A more extended mingling occurs within Configuration 3 (Fig. 2d and 4c), where: (a) globules of the annulus are mixed into the low-viscosity liquid during rapid intrusion and (b) flow instabilities (also observed by Del Bello et al., 2015) produce cyclic collapses of the low-viscosity film which, in turn, initiate a broader mingling with the high-viscosity liquid of the annulus within the tri-axial flow. The same instabilities are responsible for slug break-up and for creating partial blockages in the conduit that force the slug into smaller pockets. The effect is a pulsatory bursting with these processes coexisting. Both laboratory observations (Video V04, V07) and, particularly, CFD simulations for Stromboli (Video V06) showed that the secondary burst depths changed with time. Initially, the slug burst in the low-viscosity magma above the plug. Slug break-up then occurred at the top of the viscous annulus and secondary bubbles and transient gas pockets burst inside a region of mingled material or within the plug, with the burst depth gradually increasing. Ejected material was, therefore, scavenged at increasing depth with time, sampling different regions of the complex collapsing liquid structure. Physical changes in magma should then occur at two different scales, and the level of mingling could help in determining the flow configurations. If mixing occurs mainly during slug ascent (Configuration 3), mingling is a predominant process, likely showing, e.g., the coexistence of different vesicle populations. In contrast, the lower the mingling in the ejecta, the more restricted is the process, reflecting a possible mingling only at burst, during magma fragmentation (Configuration 2). Analysis of the mingling textures within ejecta from a strombolian eruption could, therefore, provide evidence of the near-surface flow dynamics within the conduit.

5.2. Pulsatory behaviour

At Stromboli, Gaudin et al. (2014) related individual pyroclast ejection pulses to successive pressure release pulses and sub-pulses of duration between 0.05–2 s and an average pulse rate of 7 per second, with a minimum of 3 up to 120 pulses per eruption. As a general trend, with some exceptions, the greater the number of pulses and sub-pulses, the longer the explosions, with greater gas masses involved (Gaudin et al., 2014). In our experiments, secondary bursts (pulses), followed by several partial blockages (sub-pulses) of the gas path, were achieved only in Configuration 3, with their larger number resulting from the disruption of larger gas volumes (24–49 ml). Smaller volumes (8–17 ml) generated offspring bubbles, without any sub-pulses, and shorter burst times. With these volumes scaled to the volcanic-case, CFD simulations showed the same positive correlation between volumes and number of pulses and sub-pluses as measured in the experiments. Although no formal scaling exists for these processes at laboratory-scale, the trend observed in both laboratory and CFD simulations is similar to the one derived from field observations, also suggesting the presence of a plug as a pre-requisite for pulsatory behaviour. Furthermore, CFD simulations showed that greater initial gas volume and lower viscosity of the underlying magma favour secondary bursts from offspring bubbles and sub-pulses generated by partial blockages of the conduit, while a higher viscosity led mainly to sub-pulses (restriction of gas escape pathway), with the generation of fewer, or no, secondary bubbles (blockage of gas escape pathway;

Video V06). Hence, while not measurably affecting the pre-burst processes, the viscosity of the underlying magma can noticeably influence syn-and post-burst dynamics and therefore any measured geophysical signals.

6. Conclusions

Based on scaled laboratory experiments we define a framework to describe the characteristic styles of the flow organisation involved with the ascent and burst of slugs in a rheologically stratified conduit, where a high-viscosity plug overlies a low-viscosity magma. Conduits that are fully filled with either high- or low-viscosity magma represent end-member scenarios that can be considered as infinitely thick or thin high-viscosity plugs respectively. In between, our experiments demonstrated three fundamental flow configurations, determined by the ratio of plug size and slug gas volume. In Configuration 1, the plug was sufficiently large to fully accommodate the ascending slug. In Configuration 2, a smaller plug was sufficient to accommodate the volume change due to expansion of the slug on ascent, but not the full volume of the slug. Consequently, when the slug burst at the surface of the plug, its base was still in the low-viscosity liquid. Finally, in Configuration 3, slug expansion drove an intrusion of low-viscosity liquid right through the plug, enabling slug burst to occur within the low-viscosity liquid, with the plug acting only as a region of effectively reduced conduit diameter.

We developed a model, validated with the laboratory experiments and by 3D CFD simulations at volcano-scale, to explore configuration parameter space. Our results showed how gas volume, plug thickness and plug viscosity were the key parameters controlling the transitions between different configurations; transitions were much less sensitive to properties of the underlying magma. Each configuration encompassed a variety of processes: dynamic narrowing and widening of the effective conduit, generation of instabilities along the falling liquid film, transient blockages of the slug path and slug break-up. These complexities influenced the slug ascent dynamics and gas overpressure at burst, and thus also the resulting eruptive style and, by implication, geophysical signals.

The complex flow processes can also promote magma mingling, not only by fragmentation of a rheologically layered meniscus but also through instabilities in the falling film and surrounding fluid annulus, leading to more localized or distributed regions of mingling respectively. In Configuration 3, flow instabilities cause a narrowing of the gas escape pathway causing sub-pulses within the eruption process. The flow instabilities can be sufficient to seal the gas escape pathway and cause slug break-up through the creation of transient blockages, resulting in a pulsatory, multi-bubble burst process. A widening of the conduit was needed for the slug break-up and falling film collapses, and both the viscosity of the underlying magma and the gas volume seemed to determine the frequency of pulses and sub pluses.

Our results showed how these flow configurations can influence eruption vigour, style and pyroclast properties. The configuration framework should be considered when interpreting slug-burst related geophysical signals, and points the way to more detailed links between fluid dynamic models and acoustic signals.

7. Video description

Videos **V01**, **V02**, **V03** and **V04** show the flow processes occurring during slug ascent, expansion and burst in the following experiments: (**V01**) Single and low-viscosity system, plug h = 0 cm (0D), P_a = 1 kPa, V_0 = 6 ml; (**V02**) Configuration 1, plug h = 50 cm (20D), P_a = 1 kPa, V_0 = 6 ml; (**V03**) Configuration 2, plug h = 12.5 cm (5D), P_a = 1 kPa, V_0 = 6 ml. (**V04**) Configuration 3, plug h = 12.5 cm (5D), P_a = 300 Pa, V_0 = 49 ml. Video **V05** shows the comparison between a laboratory experiment and a CFD simulation for a 10 ml slug, P_a = 3 kPa and plug h = 5 cm (2D); frame rate of the laboratory video has been accelerated to allow an easier video comparison. Video **V06** shows the comparison between three different CFD simulations at volcanic-scale, for the same gas volume, V_0 = 140 m^3, ascending in a 300-m-high volcanic conduit of radius 1.5 m, filled with magma beneath the plug (plug h = 15 m [5D]) of viscosities 50 (left), 150 (middle) and 300 (right) Pa s. Video **V0**7 contains a sequence of the bubble break-up process from an experiment of a 24 ml slug, P_a = 3 kPa and plug h = 12.5 cm (5D).

8. Acknowledgments

This research is part of A.C. PhD at Lancaster University, funded by the People Programme (Marie Curie Actions) of the European Union's Seventh Framework Programme (FP7/2007-2013) under the project NEMOH, REA grant agreement n° 289976. We thank Kathy Cashman and Sylvie Vergniolle for thorough and constructive comments that greatly improved the manuscript, and the editor Bernard Marty.

References

Blackburn, E.A., Wilson, L., and Sparks, R.S.J., 1976, Mechanisms and dynamics of strombolian activity. Journal of the Geological Society, v. 132, no. 4, p. 429–440, doi: 10.1144/gsjgs.132.4.0429.

Chouet, B., Hamisevicz, N., and Mcgetchin, T.R., 1974, Photoballistics of Volcanic Jet Activity at Stromboli, Italy. J. Geophys. Res., v. 79, no. 32, p. 4961–4976.

Chouet, B., P. Dawson, Ohminato, T., Martini, M., Saccorotti, G., Giudicepietro, F., De Luca, G., Milana, G., and Scarpa, R., 2003, Source mechanisms of explosions at Stromboli Volcano, Italy, determined from moment-tensor inversions of very-long-period data. J. Geophys. Res., 108(B1), 2019, doi:10.1029/2002JB001919.

Chouet, B., Dawson, P., Martini, M., 2008. Shallow-conduit dynamics at Stromboli Volcano, Italy, imaged from waveform inversions. In: Lane, S.J., Gilbert, J.S. (Eds.), Fluid Motions in Volcanic Conduits: A Source of Seismic and Acoustic Signals: Geol. Soc., London, Special Publications, 307, pp. 57–84.

Chouet, B. A., P. B. Dawson, M. R. James, and S. J. Lane, 2010, Seismic source mechanism of degassing bursts at Kilauea Volcano, Hawaii: Results from waveform inversion in the 10–50 s band. J. Geophys. Res., v. 115, B09311, doi:10.1029/2009JB006661.

Colò, L., Ripepe, M., Baker, D.R., and Polacci, M., 2010, Magma vesiculation and infrasonic activity at Stromboli open conduit volcano. Earth Planet. Sci. Lett., v. 292, no. 3-4, p. 274–280, doi: 10.1016/j.epsl.2010.01.018.

D’Oriano, C., Bertagnini, A., and Pompilio, M., 2011, Ash erupted during normal activity at Stromboli (Aeolian Islands, Italy) raises questions on how the feeding system works. Bull. Volcanol., v. 73, no. 5, p. 471–477, doi: 10.1007/s00445-010-0425-0.

Del Bello, E., Llewellin, E.W., Taddeucci, J., Scarlato, P., and Lane, S.J., 2012, An analytical model for gas overpressure in slug-driven explosions: Insights into Strombolian volcanic eruptions. J. Geophys. Res., v. 117, no. B2, p. B02206, doi: 10.1029/2011JB008747.

Del Bello, E., Lane, S.J., James, M.R., Llewellin, E.W., Taddeucci, J., Scarlato, P., Capponi, A., 2015, Viscous plugging can enhance and modulate explosivity of strombolian eruptions.

Earth Planet. Sci. Lett., v. 423, 1 August 2015, p. 210-218, ISSN 0012-821X, http://dx.doi.org/10.1016/j.epsl.2015.04.034.

Gaudin, D., Taddeucci, J., Scarlato, P., Moroni, M., Freda, C., Gaeta, M., and Palladino, D.M., 2014, Pyroclast Tracking Velocimetry illuminates bomb ejection and explosion dynamics at Stromboli (Italy) and Yasur (Vanuatu) volcanoes. J. Geophys. Res., v. 119, no. 7, p. 5384–5397, doi: 10.1002/2014JB011096.

Gurioli, L., Colò, L., Bollasina, A.J., Harris, A.J.L., Whittington, A., and Ripepe, M., 2014, Dynamics of strombolian explosions: inferences from field and laboratory studies of erupted bombs from Stromboli volcano. J. Geophys. Res., v. 119, 319–345, doi:10.1002/2013JB010355.

Harris, A., and M. Ripepe, 2007, Temperature and dynamics of degassing at Stromboli. J. Geophys. Res., 112, B03205, doi:10.1029/2006JB004393.

Houghton, B.F., Gonnermann, H.M., 2008, Basaltic explosive volcanism: Constraints from deposits and models. Chemie der Erde - Geochemistry, v. 68, Issue 2, 117-140, ISSN 0009-2819, http://dx.doi.org/10.1016/j.chemer.2008.04.002.

James, M.R., Lane, S.J., and Chouet, B.A., 2006, Gas slug ascent through changes in conduit diameter: Laboratory insights into a volcano-seismic source process in low-viscosity magmas. J. Geophys. Res., v. 111, no. B5, p. B05201, doi: 10.1029/2005JB003718.

James, M.R., Lane, S.J., and Corder, S.B., 2008, Modelling the rapid near-surface expansion of gas slugs in low viscosity magmas. Geological Society, London, Special Publications, v. 307, no. 1, p. 147–167, doi: 10.1144/SP307.9.

James, M.R., Lane, S.J., Wilson, L., and Corder, S.B., 2009, Degassing at low magma-viscosity volcanoes: Quantifying the transition between passive bubble-burst and Strombolian eruption: J. Volcanol. Geotherm. Res., v. 180, no. 2-4, p. 81–88, doi: 10.1016/j.jvolgeores.2008.09.002.

Jaupart, C., and Vergniolle, S., 1988, Laboratory models of Hawaiian and Strombolian eruptions. Nature, 331, 6151, 58-60

Kobayashi, T., Namiki, A., and Sumita, I., 2010, Excitation of airwaves caused by bubble bursting in a cylindrical conduit: Experiments and a model. J. Geophys. Res., doi: 10.1029/2009JB006828.

Lane, S.J., James, M.R., and Corder, S.B., 2013, Volcano infrasonic signals and magma degassing: First-order experimental insights and application to Stromboli. Earth Planet. Sci. Lett., v. 377-378, p. 169–179, doi: 10.1016/j.epsl.2013.06.048.

Lautze, N.C., and Houghton, B.F., 2005, Physical mingling of magma and complex eruption dynamics in the shallow conduit at Stromboli volcano, Italy. Geology, v. 33, no. 5, p. 425, doi: 10.1130/G21325.1.

Lautze, N.C., and Houghton, B.F., 2006, Linking variable explosion style and magma textures during 2002 at Stromboli volcano, Italy. Bull. Volcanol., v. 69, no. 4, p. 445–460, doi: 10.1007/s00445-006-0086-1.

Llewellin, E.W., Del Bello, E., Taddeucci, J., Scarlato, P., and Lane, S.J., 2012, The thickness of the falling film of liquid around a Taylor bubble. Proc. R. Soc., Math. Phys. Eng. Sci., v. 468, no. 2140, p. 1041–1064, doi: 10.1098/rspa.2011.0476.

McGreger, A.D., and Lees, J.M. 2004, Vent discrimination at Stromboli volcano, Italy. J. Volcanol. Geotherm. Res., v. 137, 169–185, doi: http://dx.doi.org/10.1016/j.jvolgeores.2004.05.007.

Mori, T., and Burton, M., 2009, Quantification of the gas mass emitted during single explosions on Stromboli with the SO2 imaging camera. J. Volcanol. Geotherm. Res., 188(4), 395-400, doi:10.1016/j.jvolgeores.2009.10.005

Parfitt, E.A., and Wilson, L., 1995, Explosive volcanic eruptios: IX The transition between Hawaiian-style lava fountaining and Strombolian explosive activity. Geophys. J. Int., 121, 226-232

Parfitt, E. A., 2004, A discussion of the mechanisms of explosive basaltic eruptions. Journal of Volcanology and Geothermal Research, 134(1–2), 77–107, doi:10.1016/j.jvolgeores.2004.01.002.

Polacci, M., Baker, D. R., Mancini, L., Favretto, S., and Hill, R.J., 2009, Vesiculation in magmas from Stromboli and implications for normal Strombolian activity and paroxysmal explosions in basaltic systems. J. Geophys. Res., v. 114, B01206, doi: 10.1029/2008JB005672.

Ripepe, M., and Marchetti, E., 2002, Array tracking of infrasonic sources at Stromboli volcano. Geophys. Res. Lett., 29(22), 33-1. doi: 10.1029/2002GL015452

Seyfried, R., and Freundt, A., 2000, Experiments on conduit flow and eruption behaviour of basaltic volcanic eruptions. J. Geophys. Res., v. 105, no. B10, p. 727-740, doi: 10.1029/2000JB900096.

Taddeucci, J., Scarlato, P., Capponi, A., Del Bello, E., Cimarelli, C., Palladino, D.M., and Kueppers, U., 2012, High-speed imaging of Strombolian explosions: The ejection velocity of pyroclasts. Geophys. Res. Lett., v. 39, no. 2, L02301, doi: 10.1029/2011GL050404.

Vergniolle, S., and Jaupart, C., 1986, Separated two-phase flow and basaltic eruptions. J. Geophys. Res., 91(B12), 12842-12860.

Vergniolle, S., and Brandeis, G., 1996, Strombolian explosions 1. A large bubble breaking at the surface of a lava column as a source of sound. J. Geophys. Res., v. 101, no. B9, p. 433–447.

Vergniolle, S., Brandeis, G., and Mareschal, J.C., 1996, Strombolian explosions 2. Eruption dynamics determined from acoustic measurements. J. Geophys. Res., v. 101, no. B9, p. 449-466.

Vergniolle, S., 1998, Modelling two-phase flow in a volcano. In Proc. 13th Australasian Fluid Mech. Conf. Aristoc. Offset, Monash University, Melbourne, 647-650.

White, E. T., and Beardmore, R. H., 1962, The velocity of rise of single cylindrical air bubbles through liquids contained in vertical tubes. Chem. Eng. Sci., v. 17, p. 351–361.

Table 1 Comparison of experimental parameters from this study and from Del Bello et al. (2015) and scaling to the volcanic case

Materials	Water[a]	Silicone oil[b]	Castor oil[a-b]	Underlying magma[e]	Plug[e]
Conduit radius, r_c (m)	0.0125			2.5	
Density (kg/m^3)	1000	990	961	900	1300
Viscosity (Pa s)	0.001	0.1	1	50-300	10000-50000
Inverse viscosity, N_f	12380	122	12	630-105	4.5-0.91
Film cross section, A'[c]	0.16	0.41	0.52	0.26-0.36	0.53-0.54
Dimensionless film, λ'[d]	0.08	0.23	0.31	0.14-0.24	0.32-0.32
Film thickness, λ (m)	0.001	0.0029	0.0039	0.35-0.60	0.80-0.81
Slug radius, r_s (m)	0.011	0.0095	0.0085	1.89-2.14	1.67-1.68
Viscosity contrast	1000	10		33-1000	

[a] used in Del Bello et al. (2015)
[b] used in this study
[c] calculated from equation (28) in Del Bello et al. (2012)
[d] calculated from equation (4.2) in Llewellin et al. (2011)
[e] viscosity and densisty data reported in Gurioli et al. (2014)

Table 2 Model notation

geometrical parameters	
P_a	ambient pressure
P_0	initial bubble pressure
P	bubble pressure
L_0	initial bubble length
L	bubble length
h'_1	initial height of low-viscosity liquid above the slug
h'_3	initial height of the plug
h_1	height of low-viscosity liquid above the bubble
h_2	height of low-viscosity intrusion
h_3	depth from the plug top to the intrusion
$v_s t$	depth from the bubble base to the tube base
r_c	tube radius
r_s	bubble radius
r_p	viscous annulus radius
r_φ	intrusion radius
μ_1	viscosity of the liquid beneath the plug
μ_2	plug viscosity
ρ_1	low-viscosity liquid density
ρ_2	plug density

Figure 1

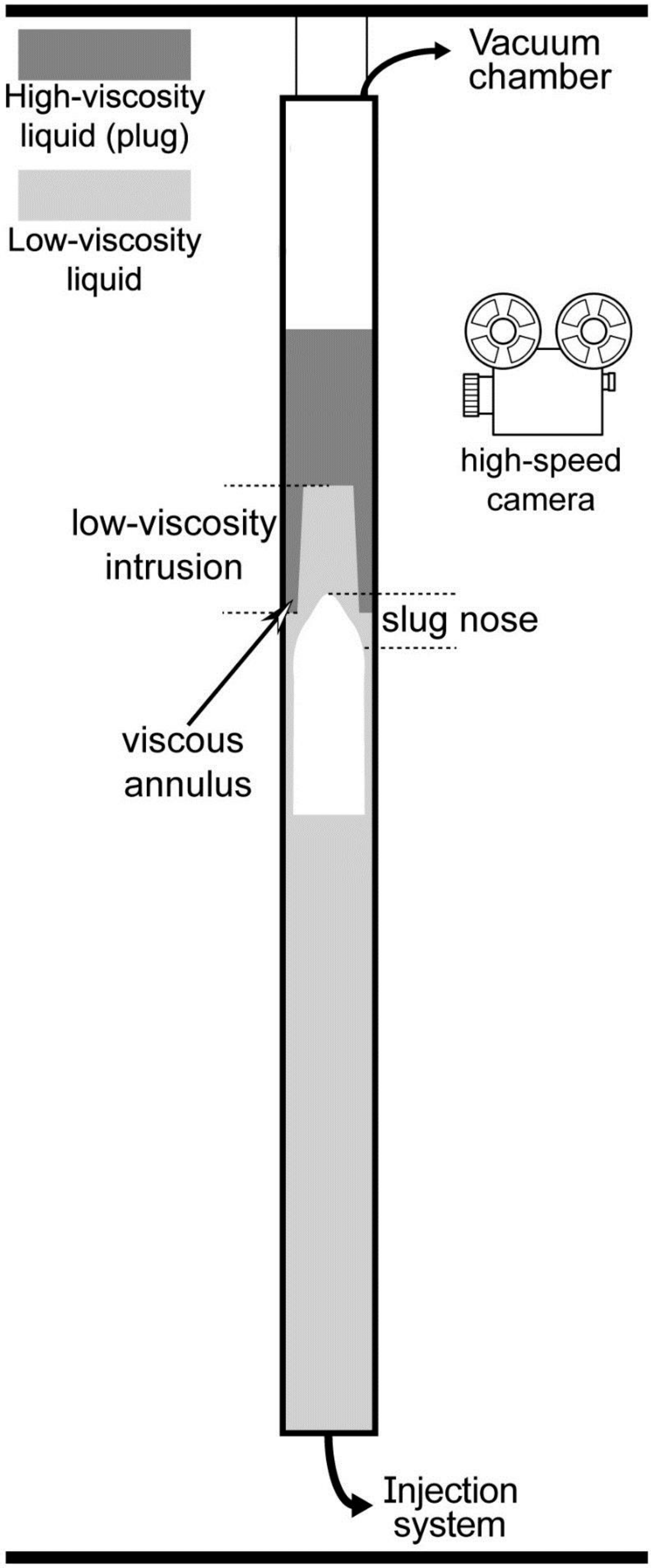

Vacuum chamber
High-viscosity liquid (plug)
Low-viscosity liquid
high-speed camera
low-viscosity intrusion
slug nose
viscous annulus
Injection system

Figure 2

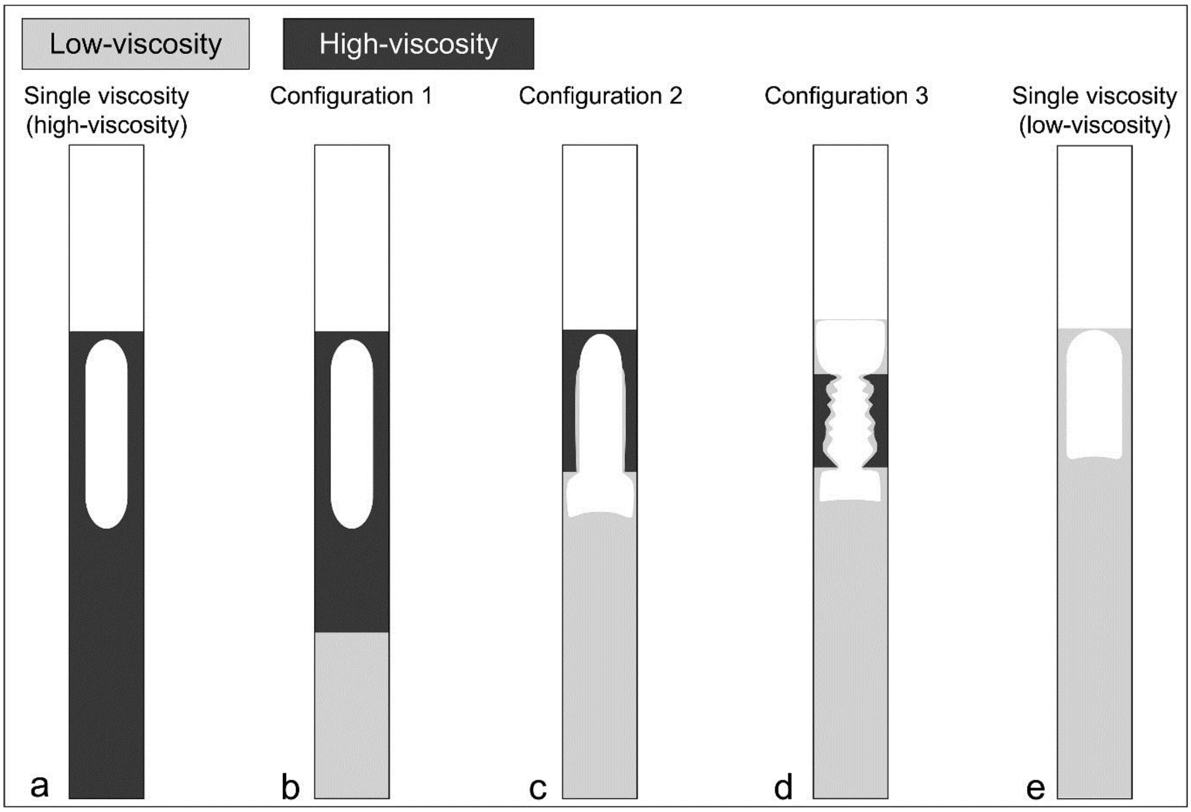
Low-viscosity
High-viscosity
Single viscosity (high-viscosity)
Configuration 1
Configuration 2
Configuration 3
Single viscosity (low-viscosity)
a
b
c
d
e

Figure 3

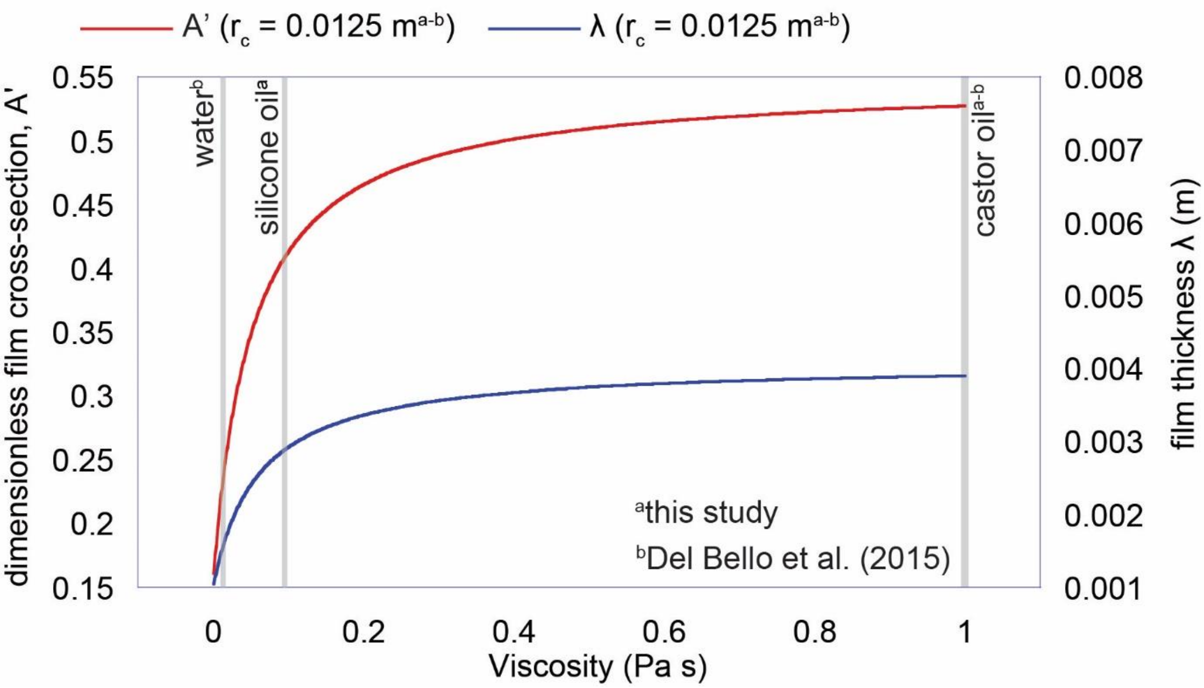

A' (r_c = 0.0125 m^a-b)
λ (r_c = 0.0125 m^a-b)
dimensionless film cross-section, A'
film thickness λ (m)
Viscosity (Pa s)
water^b
silicone oil^a
castor oil^a-b
^a this study
^b Del Bello et al. (2015)
0.55
0.5
0.45
0.4
0.35
0.3
0.25
0.2
0.15
0.008
0.007
0.006
0.005
0.004
0.003
0.002
0.001
0
0.2
0.4
0.6
0.8
1

Figure 4

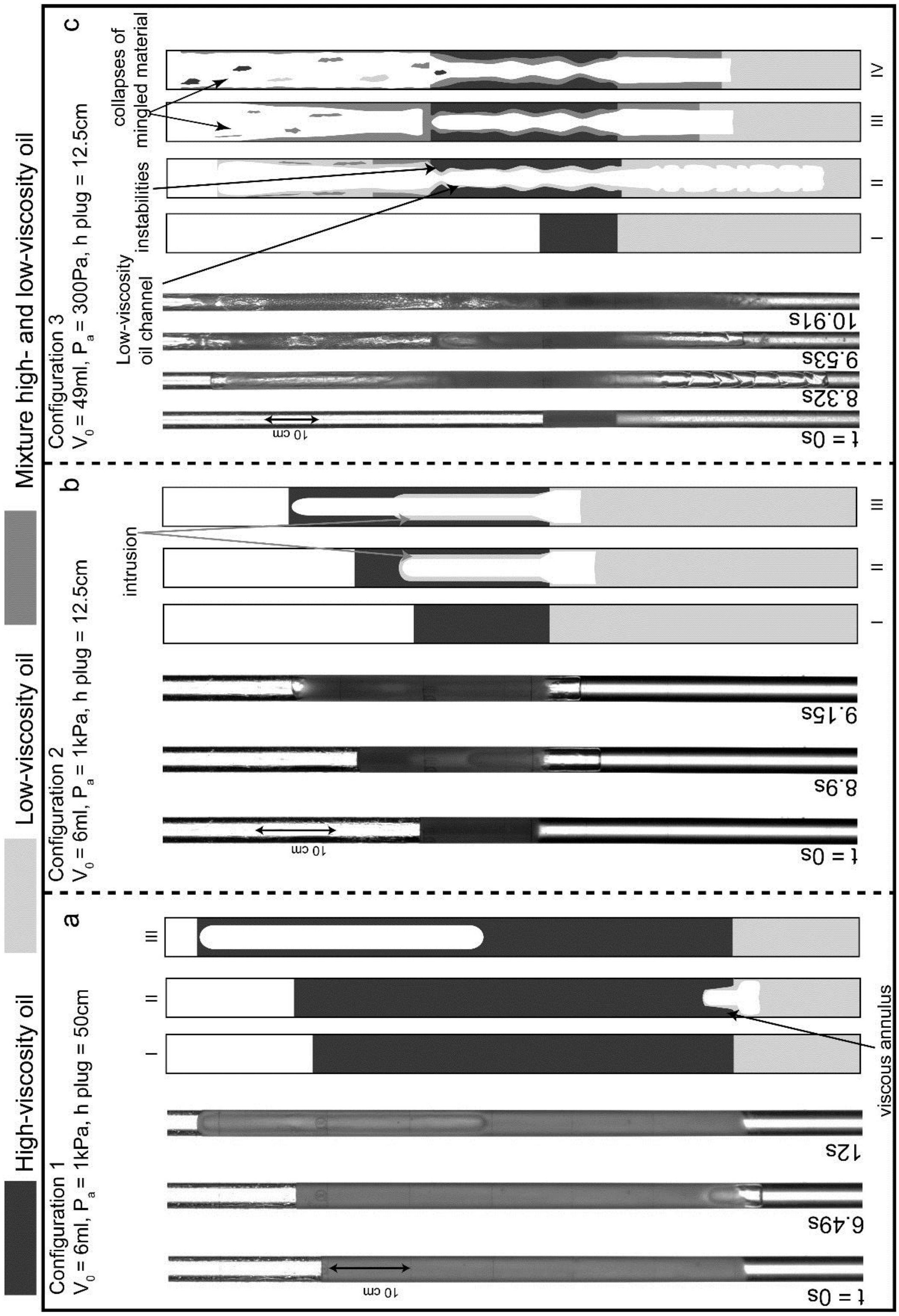

High-viscosity oil
Low-viscosity oil
Mixture high- and low-viscosity oil
a
Configuration 1
V_0 = 6ml, P_a = 1kPa, h plug = 50cm
t = 0s
6.49s
12s
10 cm
I
II
III
viscous annulus
b
Configuration 2
V_0 = 6ml, P_a = 1kPa, h plug = 12.5cm
t = 0s
8.9s
9.15s
10 cm
intrusion
I
II
III
c
Configuration 3
V_0 = 49ml, P_a = 300Pa, h plug = 12.5cm
t = 0s
8.32s
9.53s
10.91s
10 cm
Low-viscosity oil channel
instabilities
collapses of mingled material
I
II
III
IV

Figure 5

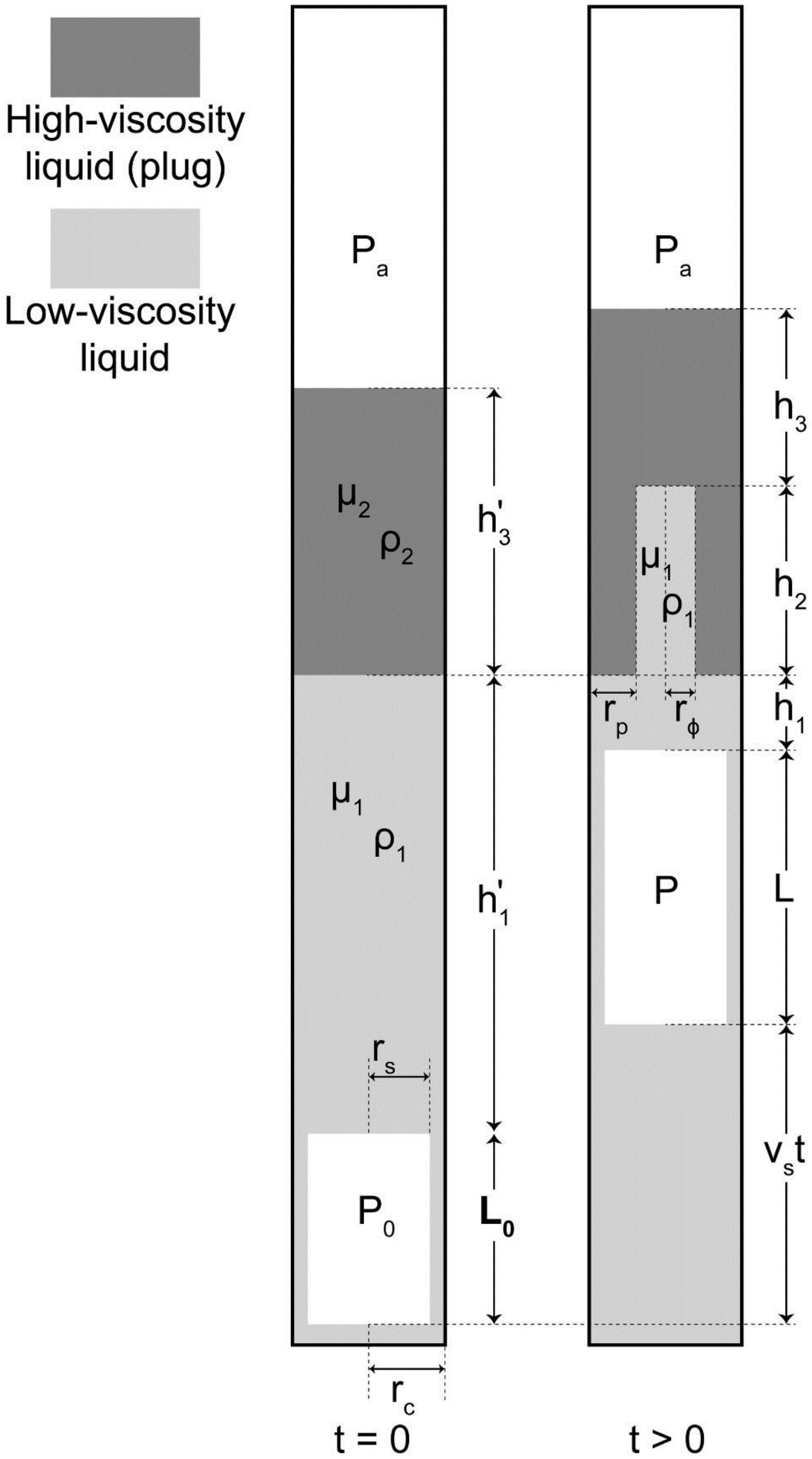
High-viscosity liquid (plug)
Low-viscosity liquid
P_a
P_a
μ_2
ρ_2
h'_3
μ_1
ρ_1
h'_1
r_s
P_0
L_0
r_c
h_3
μ_1
ρ_1
h_2
r_p
r_ϕ
h_1
P
L
$v_s t$
t = 0
t > 0

Figure 6

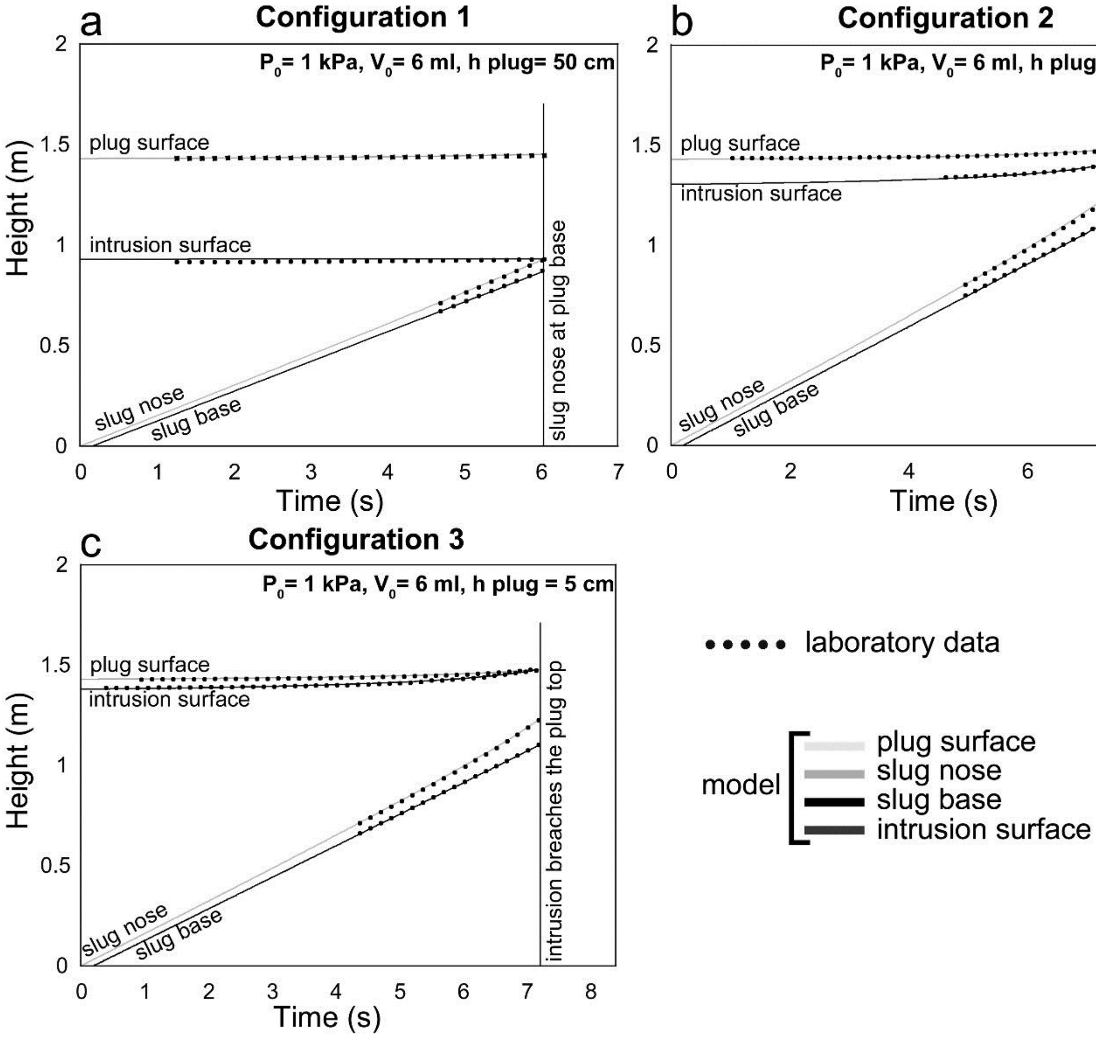
a
Configuration 1
P0= 1 kPa, V0= 6 ml, h plug= 50 cm
Height (m)
Time (s)
plug surface
intrusion surface
slug nose
slug base
slug nose at plug base
b
Configuration 2
P0= 1 kPa, V0= 6 ml, h plug = 12.5 cm
plug surface
intrusion surface
slug nose
slug base
slug nose at plug base
Time (s)
c
Configuration 3
P0= 1 kPa, V0= 6 ml, h plug = 5 cm
Height (m)
plug surface
intrusion surface
slug nose
slug base
intrusion breaches the plug top
Time (s)
laboratory data
model
plug surface
slug nose
slug base
intrusion surface

Figure 7

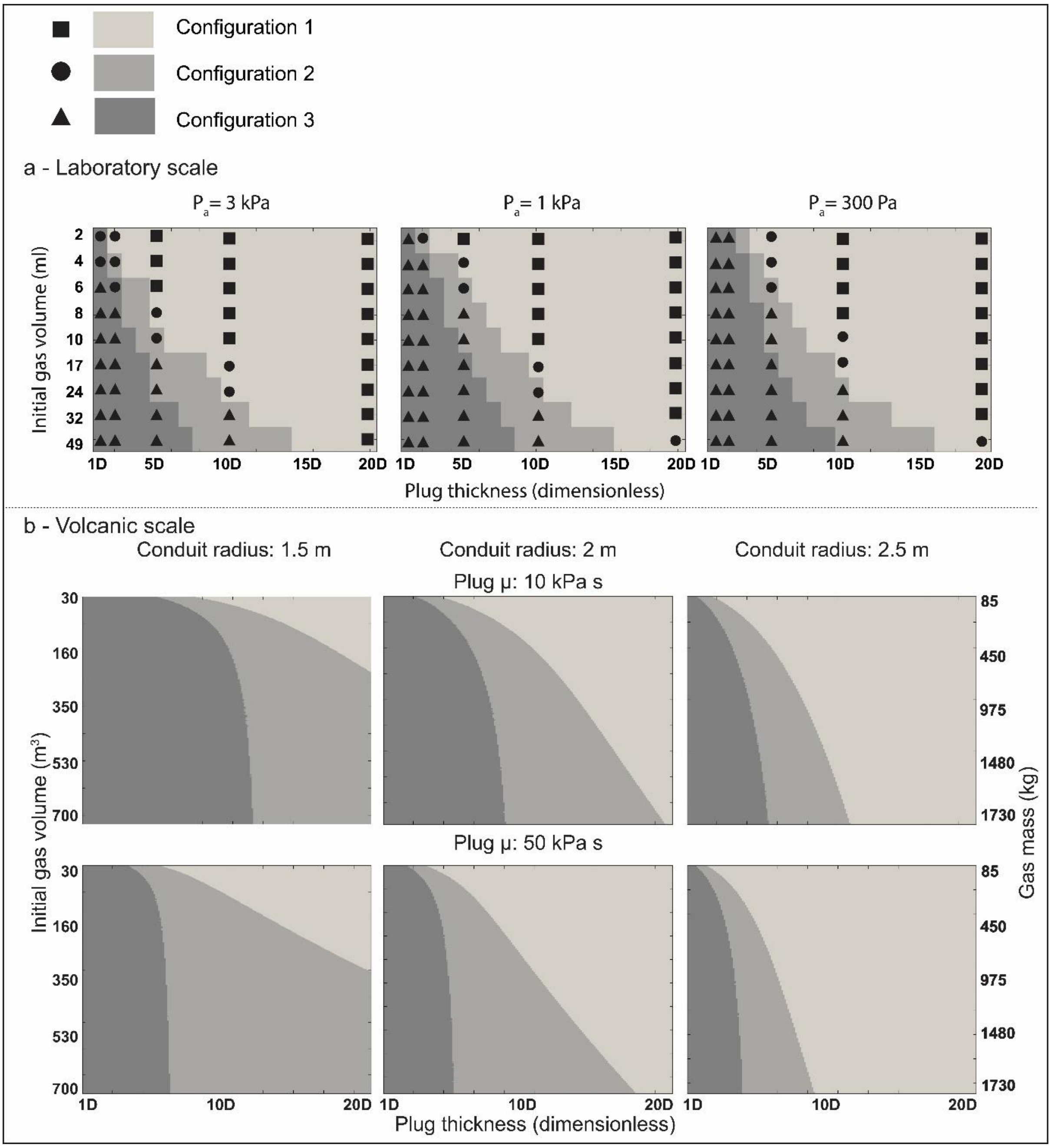

Configuration 1
Configuration 2
Configuration 3
a - Laboratory scale
P_a = 3 kPa
P_a = 1 kPa
P_a = 300 Pa
Initial gas volume (ml)
2
4
6
8
10
17
24
32
49
1D
5D
10D
15D
20D
Plug thickness (dimensionless)
b - Volcanic scale
Conduit radius: 1.5 m
Conduit radius: 2 m
Conduit radius: 2.5 m
Plug µ: 10 kPa s
Plug µ: 50 kPa s
Initial gas volume (m³)
30
160
350
530
700
Gas mass (kg)
85
450
975
1480
1730
1D
10D
20D
Plug thickness (dimensionless)

Figure 8

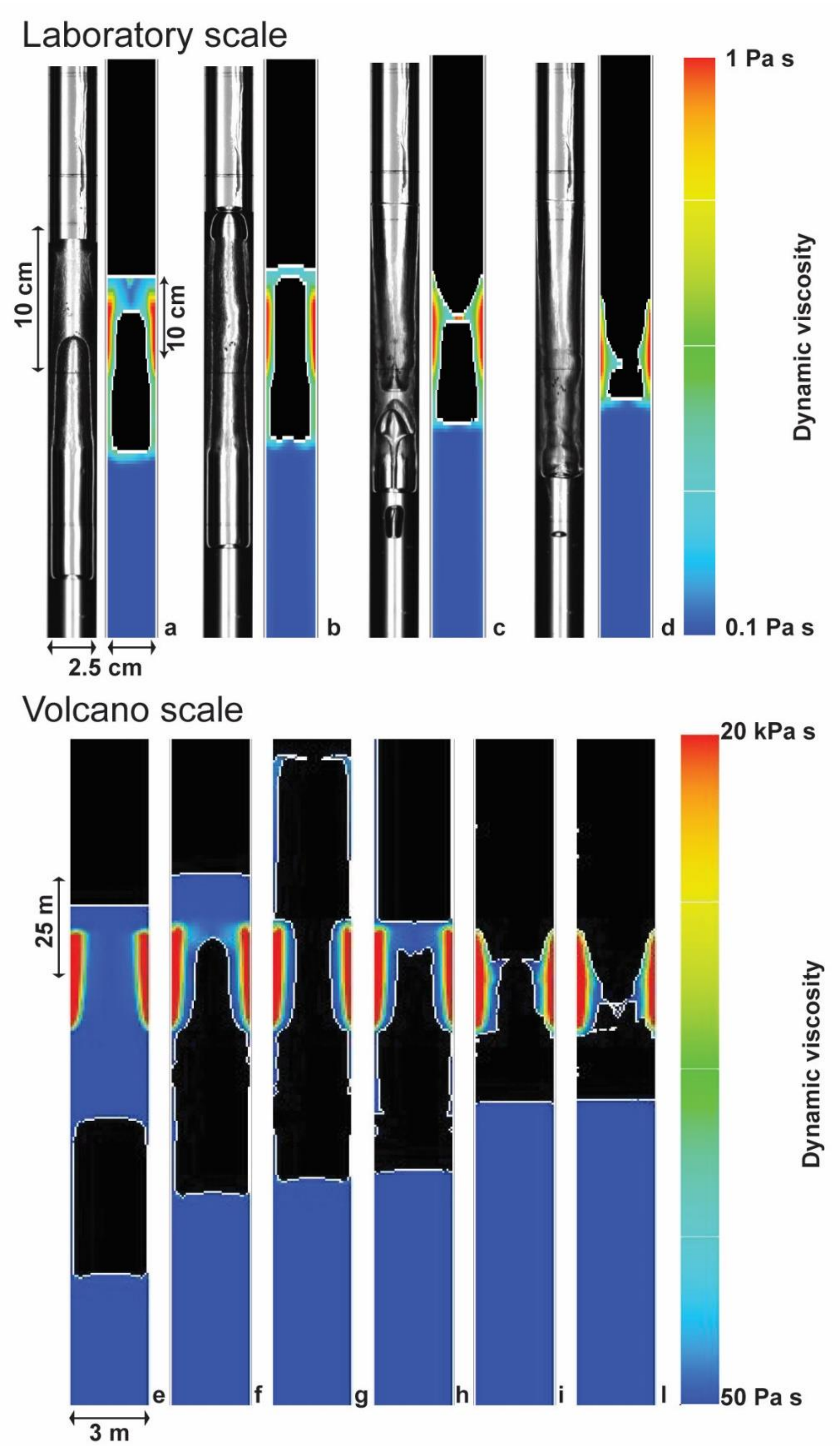

Laboratory scale
10 cm
10 cm
a
b
c
d
2.5 cm
1 Pa s
Dynamic viscosity
0.1 Pa s
Volcano scale
25 m
e
f
g
h
i
l
3 m
20 kPa s
Dynamic viscosity
50 Pa s

Figure Captions

Figure 1. The experimental apparatus comprised a 3-m-high vertical tube, with a diameter *D* of 0.025 m, connected to a vacuum chamber and a gas injection system. Scaling considerations dictated that experimental ambient pressure was varied between 3 kPa, 1 kPa and 300 Pa. Slug ascent, expansion and burst through the experimental liquids were imaged with a high-speed camera at 300 fps. As a slug ascended and expanded in the tube, it drove an intrusion of the underlying low-viscosity liquid into the plug, forming a low-viscosity channel (**low-viscosity intrusion**). The intrusion displaced and spread the high-viscosity liquid along the tube wall, creating a high-viscosity annulus (**viscous annulus**) that, in turn, enclosed the intrusion.

Figure 2. Experimentally informed conceptual sketches of tubes filled with (**a**) high-viscosity and (**e**) low-viscosity liquid represent the configuration end-members that sandwiched three main flow configurations for the two-layer system. (**b**) Configuration 1: the viscous plug volume fully accommodates the gas slug. (**c**) Configuration 2: the plug volume cannot accommodate both the low-viscosity intrusion and the slug. At burst, the slug nose and main body are in the plug, whilst the base is still in the low-viscosity liquid. (**d**) Configuration 3: slug expansion drives the intrusion of low-viscosity liquid through the plug, extruding a low-viscosity layer above the plug in which the slug burst. Instabilities develop as the slug passes through the annulus into the extruded low-viscosity layer.

Figure 3. Variations of the dimensionless film cross section *A'* (calculated from equation (28) in Del Bello et al. 2012) and thickness of the falling liquid film (m), λ, as function of viscosity for a tube radius of 0.0125 m; shaded areas highlight the values for water (μ = 0.001 Pa s, ρ = 1000 kg/m^3; used in Del Bello et al. 2015), silicone oil (μ = 0.1 Pa s, ρ = 990 kg/m3;

this study) and castor oil (μ = 1 Pa s, ρ = 961 kg/m^3; both this study and Del Bello et al. 2015).

Figure 4. Still frames and interpretative sketches from selected experiments representative of the identified flow configurations are shown. (**a**) Configuration 1: as the slug rose, gas expansion drove the intrusion of low-viscosity liquid into the plug (6.49 s); once the transition between the liquids was complete, the slug was fully accommodated within the plug (12 s). (**b**) Configuration 2: the slug exploited the low-viscosity intrusion, enclosed within the viscous annulus, to ascend through the plug (8.9 s). This tri-axial flow comprises ascending gas, descending low-viscosity liquid and, at flow timescale, relatively stationary high-viscosity liquid. At burst: (i) the slug nose was within the viscous plug, (ii) the low-viscosity film and the viscous annulus surrounded the slug main body (tri-axial flow), and (iii) the slug base remained in the low-viscosity liquid below the plug (annulus) base (9.15 s). (**c**) Configuration 3: the low-viscosity intrusion breached the plug top, and the slug burst into the extruded low-viscosity layer (8.32 s); instabilities formed and propagated along the falling film, leading to bubble break-up, partial blockage of the conduit and mixing between liquids (9.53 s). At burst, globules of this mixture fell back on the liquid surface (10.91 s).

Figure 5. The 1D model geometry for a gas slug ascending in a low-viscosity liquid overlaid by a high-viscosity liquid is shown. White regions represent the gas bubble, while grey-scale regions the liquids. See Table 2 for a complete geometrical notation.

Figure 6. Comparison of slug ascent profiles measured from laboratory video (symbols) and the 1D model (lines) for each flow configuration. A 6 ml slug ascends in a liquid column overlain by a plug of 50 cm (Configuration 1; **a**), 12.5 cm (Configuration 2; **b**) and 5 cm (Configuration 3; **c**) with a P_a = 1 kPa. In all cases the variations in position of the plug surface, intrusion surface, slug nose and slug base are well reproduced. For Configuration 3

(**c**), the intersection between the plug and intrusion curves indicates that the low-viscosity liquid breached the plug surface. The comparison with the experimental data is limited up to the moment the simulation stopped. Note that video data for the slug ascent are not available for heights < ~0.5 above the apparatus base, because of the camera field of view.

Figure 7. (a) Comparison between experimental fluid configurations (symbols) and configurations forecasted by the 1D model (shaded regions) is shown as a function of initial gas volume (ml) and plug thickness (dimensionless), for ambient gas pressures of 3 kPa (left), 1 kPa (middle) and 300 Pa (right). (**b**) Flow configurations forecast by the 1D model for an idealized volcanic scenario are shown, for a plug viscosity of 10 kPa s (upper row) and 50 kPa s (lower row), and as function of initial gas volume (m^3), or gas mass (kg; right axis), plug thickness (dimensionless) and volcanic conduit radii of 1.5 (left), 2 (middle) and 2.5 (right) m; the configuration distribution is insensitive to the viscosity of magma beneath the plug within the limit 50-500 Pa s.

Figure 8. (upper panel) Still frames from a laboratory experiment and 3D CFD simulation for a 10 ml slug, expanding in a P_a = 3 kPa and a plug h = 12.5 cm (Configuration 3). The CFD simulation reproduced experimental observation well, including the variations in slug shape, intrusion dynamics, burst dynamics and bubble breakup process (see also Video V05). Note the asymmetry in panels **c** and **d** that demonstrate the requirement for full 3D simulation. (**lower panel**) Still frames from a 3D CFD simulation at volcanic-scale. Input parameters are V_0 = 140 m^3, $P_a = 10^5$ Pa, μ_{magma} = 50 Pa s, μ_{plug} = 20 kPa s, r_c = 1.5 m, column h = 200 m, conduit radius r_c = 1.5 m, conduit h = 300 m, and plug h = 15 m. Note the visible asymmetry that develops once instabilities arise from panel **g** onward, underscoring the requirement for a 3D approach once dynamic instability develops.